Near-Earth plasma sheet azimuthal pressure gradient and associated auroral development soon before substorm onset

X. Xing,[1] L. R. Lyons,[1] Y. Nishimura,[1,2] V. Angelopoulos,[3] E. Donovan,[4] E. Spanswick,[4] J. Liang,[4] D. Larson,[5] C. Carlson,[5] and U. Auster[6]

Received 7 February 2011; revised 25 March 2011; accepted 7 April 2011; published 7 July 2011.

[1] The azimuthal plasma pressure gradient in the near-Earth plasma sheet makes crucial contributions to field-aligned current (FAC) formation. Numerical simulations and statistical observations have shown that a plasma pressure peak tends to build up in the premidnight region of the near-Earth plasma sheet during the substorm growth phase owing to enhanced magnetic drift. This leads to azimuthal pressure gradients in this region. The temporal variation of the azimuthal pressure gradient may provide an indication for the FAC variations associated with the substorm growth phase and may set up a plasma sheet precondition for the substorm onset being triggered near this region. We take advantage of two of the Time History of Events and Macroscale Interactions during Substorms (THEMIS) spacecraft separated azimuthally near the orbit apogee and investigate the azimuthal plasma pressure gradient before substorm onset in the R ~10–12 R_E region. Equatorial plasma pressure is estimated by removing the curvature force effect. Five events with the spacecraft footprints mapped very close to the aurora onset region were selected. These events show substantial duskward pressure gradient enhancement 1–5 min before onset. The onset arc, which results from enhanced energetic electron precipitation, was found to intensify simultaneously with the pressure gradient enhancement before onset breakup occurs. Since the energy and energy flux of precipitating electrons reflect the upward FAC strength, these results indicate that the duskward azimuthal pressure gradient enhancement is associated with enhanced upward FAC during the late growth phase and leads to the intensification of the onset auroral arc soon before it breaks up. It is possible that this pressure gradient enhancement may lead to ballooning mode instability and thus substorm onset along the intensifying arc.

Citation: Xing, X., L. R. Lyons, Y. Nishimura, V. Angelopoulos, E. Donovan, E. Spanswick, J. Liang, D. Larson, C. Carlson, and U. Auster (2011), Near-Earth plasma sheet azimuthal pressure gradient and associated auroral development soon before substorm onset, *J. Geophys. Res.*, *116*, A07204, doi:10.1029/2011JA016539.

1. Introduction

[2] The substorm onset triggering mechanism has been a key question since the beginning of substorm research, but general agreement on the timing sequence leading to substorm onset has yet to reach a conclusive agreement despite over 40 years of debate [e.g., *McPherron et al.*, 1973; *Angelopoulos et al.*, 2008; *Lui*, 2008]. Recently, *Nishimura et al.* [2010a], *Lyons et al.* [2010], and *Xing et al.* [2010] presented evidence for a new idea of the preonset sequence starting with a poleward boundary intensification (PBI) associated with local reconnection occurring near the magnetic separatrix. Reduced entropy flow channels formed after the PBIs then convected approximately earthward into the near-Earth plasma sheet associated with approximately equatorward moving aurora streamers. Substorm onset occurs following the low-entropy plasma intrusion to the near-Earth plasma sheet. However, some reduced entropy flow channels associated aurora streamers reach the preexisting aurora arc near the equatorward boundary of the auroral oval but do not lead to onset [*Xing et al.*, 2010; *Nishimura et al.*, 2010b], consistent with what was found earlier by *Ohtani et al.* [2002] in a case study. *Xing et al.* [2010] suggested that necessary preonset conditions, such as enhanced plasma pressure and pressure gradient, have to be built up in the near-Earth plasma sheet.

[3] During the substorm growth phase, the statistical plasma sheet pressure is found to be higher than during quiet times owing to the enhanced earthward convection [*Wang*

[1]Department of Atmospheric and Oceanic Sciences, University of California, Los Angeles, California, USA.
[2]Solar-Terrestrial Environment Laboratory, Nagoya University, Nagoya, Japan.
[3]IGPP/ESS, University of California, Los Angeles, California, USA.
[4]Department of Physics and Astronomy, University of Calgary, Calgary, Alberta, Canada.
[5]Space Sciences Laboratory, University of California, Berkeley, California, USA.
[6]Institut für Geophysik und Extraterrestrische Physik, Technische Universität Braunschweig, Braunschweig, Germany.

0148-0227/11/2011JA016539

et al., 2004a; *Miyashita et al.*, 2009]. The enhanced magnetic drift in the near-Earth plasma sheet gives an enhanced dawn-dusk pressure asymmetry leading to increased azimuthal pressure gradient [*Lui and Rostoker*, 1991; *Wang et al.*, 2004a, 2004b, 2007; *Gkioulidou et al.*, 2009], which increases and redistributes the Region 2 field-aligned currents (FACs) [*Vasyliunas* 1970; *Lyons et al.*, 2003; *Stepanova et al.*, 2004; *Gkioulidou et al.*, 2009] relative to the quiet time background FAC [*Wing and Newell*, 1998; *Xing et al.*, 2009]. A well-developed Region 2 FAC system in the near-Earth plasma sheet has been suggested to play a crucial role in substorm physics [*Lyons et al.*, 2009]. The changing of the FAC distribution may feed back to the plasma sheet convection via magnetosphere-ionosphere electrodynamic coupling, and thus affect the formation of the Harang reversal, which is found to be closely related to substorm onsets [*Bristow et al.*, 2001, 2003; *Bristow and Jensen*, 2007; *Zou et al.*, 2009]. Therefore, the evolution of the azimuthal pressure gradient during the growth phase may set up an important precondition for the initiation of substorm onset instabilities.

[4] The large-scale azimuthal pressure gradient in the near-Earth plasma sheet has been estimated from statistical observations of the pressure distribution within the plasma sheet [*Shiokawa et al.*, 1998; *Wang et al.*, 2007], and from low-altitude observations mapped to the equatorial plane [*Wing and Newell*, 1998, 2000] sorted by solar wind conditions and activity levels. However, the temporal evolutions of the pressure gradient during the growth phase cannot be deduced from these statistics. *Miyashita et al.* [2009] studied the plasma sheet pressure evolution during the several minutes time period before the substorm onset, which also reveals some information about the pressure gradient change, but they did not consider the pressure gradient evolution or relations to the onset location.

[5] In situ observations at different locations in the near-Earth plasma sheet are desirable for examining pressure gradient evolution, as was performed by *Xing et al.* [2009] for the quiet time plasma sheet. In the present study, we adopt the method used by *Xing et al.* [2009] by taking advantage of two of the THEMIS [*Angelopoulos*, 2008] spacecraft D and E, which have overlapping orbits in the near-Earth plasma sheet and align azimuthally near the orbit apogee every day, to analyze the azimuthal pressure gradient evolution during the growth phase. The pressure gradient changes very close to the substorm onset location will be investigated in detail.

[6] In section 2, the event selection criteria and the basic data information will be presented. In section 3, we will first introduce the method used to estimate the equatorial plasma pressure from observations in the near-Earth plasma sheet, where pressure balance in Z_{GSM} may not hold, and then analyze the selected events in detail. The results will be summarized in section 4.

2. Data Set

[7] We collected observations during the 2009 THEMIS tail season for substorms occurring while the spacecraft THD and THE were within 1.5 h of the orbit apogee so that the radial difference between the two spacecraft was small ($dR/R < 0.02$). Rough estimation form the *Tsyganenko and Mukai* [2003] plasma sheet pressure model under different solar wind conditions suggests that the pressure radial difference within $dR/R < 0.02$ at $R \sim 10\ R_E$ is usually smaller than 3% of the local pressure. Thus we take the measured pressure gradient near orbit apogee to be mainly the azimuthal component. We used only the 2009 tail season data because the spacecraft THA was above/underneath one of THD and THE in Z_{GSM} during the orbit apogee during this year, and we used THA for removing the magnetic tension effect while calculating equatorial plasma pressure (see section 3.1). Substorm onsets are selected to be the auroral breakup onset, which are identified using the THEMIS ground-based All-Sky Imagers (ASIs) by abrupt aurora brightening followed by poleward expansion. The spacecraft THD and THE are both required to have a close equatorial passing (magnetic $\beta > 20$; see *Lui et al.* [1992]) during or before the growth phase field line stretching starts, which is important for accurately calculating the equatorial plasma pressure. The events with spacecraft footprints mapped to the vicinity of the aurora onset breakup are selected for analysis in section 3. While the events selected under these criteria are limited in number, these conditions limit the ambiguities in determining the azimuthal gradient of the equatorial plasma pressure near the onset location.

[8] Both the Electrostatic Analyzer (ESA) [*McFadden et al.*, 2008] and Solid State Telescope (SST) particle detectors, which cover the particle energy range from 5 eV to 6 MeV for ions and 5 eV to 1 MeV for electrons, were used for particle pressure measurements. The magnetic field and electric field data are taken from the Fluxgate Magnetometer (FGM) [*Auster et al.*, 2008]. The aurora data are obtained from THEMIS All-Sky Imagers (ASIs) [*Mende et al.*, 2008]. Spacecraft footprints ranges are roughly estimated by mapping to the ionospheric E region using the T96 magnetic field model [*Tsyganenko and Stern*, 1996] with the different input solar wind conditions referred from OMNIWeb and WDC-C2 for Geomagnetism, Kyoto, and the Tsyganenko 2001 magnetic field model [*Tsyganenko* 2002a, 2002b] using instantaneous solar wind conditions as a comparison.

3. Data Analysis

3.1. Vertical Pressure Balance Estimation

[9] Vertical pressure balance in Z_{GSM} is believed to be a good assumption in stretched tail configurations. However, this condition may be broken in the plasma sheet transition region where the magnetic field lines are less stretched [*Erickson and Wolf*, 1980]. *Xing et al.* [2009] compared the magnetic pressure and tension force in different 2-D magnetic field line configurations and found that the tension force is much smaller than the magnetic pressure in a stretched magnetic field, and comparable but still smaller than the magnetic pressure in near-dipolar magnetic field. The THEMIS spacecraft locations during the 2009 tail season makes calculating the tension force possible under the assumption that the magnetic field dawn-dusk variation is smaller than the radial variation. The equatorial plasma pressure can be estimated using equation (1) (GSM coordinate are used throughout) by vertically projecting the spacecraft location at (x_0, y_0, z_1) to the equatorial plane at $(x_0, y_0, 0)$.

$$P_{eq} = P_{th-1} + \frac{B_{x-1}^2 + B_{y-1}^2}{2\mu_0} - \frac{1}{\mu_0}\int_0^{z_1} \frac{\partial B_z}{\partial x} B_x dz \qquad (1)$$

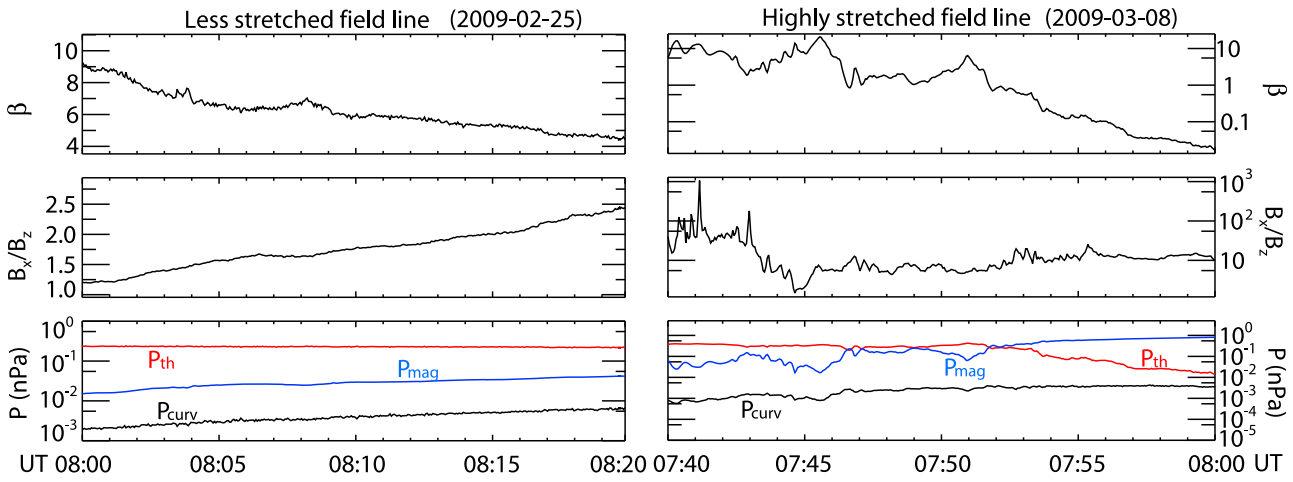

Figure 1. (top) Magnetic β, (middle) B_x/B_z, and (bottom) the three terms on the right-hand side of equation (1) with thermal pressure (red curves), magnetic pressure (blue curves), and tension force (black curves). (left) Less stretched field line. (right) Highly stretched field line.

P_{eq} represents estimated equatorial plasma pressure. P_{th-1} is the measured thermal pressure. $B_{x/y-1}$ represent the x and y components of the measured magnetic field. The third term representing the curvature force is the factor that can break down the vertical pressure balance assumption in the tail transition region and affect the accuracy of the pressure gradient calculation. By taking advantage of the third THEMIS probe THA located at (x_0, y_0, z_2), which is above/below THD or THE located at (x_0, y_0, z_1) and have very close projection in the equatorial plane. $\partial B_x/\partial x$ in the curvature term can be calculated by equation (2).

$$\frac{\partial B_x}{\partial x} = \frac{\left(2\mu_0(P_{th-1} - P_{th-2}) + \left(B^2_{x-1} + B^2_{y-1} - B^2_{x-2} - B^2_{y-2}\right)\right)}{2(B_{x-1}Z_1 - B_{x-2}Z_2)} \quad (2)$$

Assuming that $\partial B_x/\partial x$ is only a function of Z_{GSM}, and the plasma sheet is symmetric across the neutral sheet, the curvature term can be calculated from data directly.

[10] Figure 1 shows an example of the curvature force estimation for different field line configurations. The magnetic $\beta > 1$ in Figure 1 (top left) and the ratio of B_x/B_z around 1 in Figure 1 (middle left) suggest a plasma sheet measurement in a less stretched magnetic field line configuration than that in Figure 1 (middle right), whereas smaller magnetic β associated with large B_x/B_z indicates a more stretched field. Figure 1 (bottom left) also displays the three terms in the right-hand side of equation (1) with the thermal pressure in red, the magnetic pressure in blue, and the curvature term in black. The curvature force is about one order smaller than the magnetic force. In the highly stretched field line in Figure 1 (right), where the spacecraft gradually moved away from the central plasma sheet owing to the field line stretching, the curvature force is roughly two orders smaller than the magnetic force. These are consistent with the results in the work of *Xing et al.* [2009] that the curvature force is always much smaller than the magnetic force, particularly in the growth phase stretched field lines. However, because the azimuthal pressure gradient is small at $R \sim 11\ R_E$ [*Xing et al.*, 2009], and the two spacecraft may move to different vertical distance from the neutral sheet during stretching, ignoring the curvature force can still affect the accuracy of the pressure gradient calculation. Thus the curvature effect has been removed in the analysis presented here.

3.2. Case Studies of Azimuthal Pressure Gradient Near the Plasma Sheet Onset Region Prior to Onset

[11] We have identified five good conjunction events during the 2009 THEMIS tail season, for which well-defined substorms occurred while the THD and THE were close to the orbit apogee, mapped close to the onset location, and had equatorial passing before or during the growth phase. All of these events show a substantial duskward pressure gradient enhancement 1–5 min before the substorm onset associated with an intensification of a fine aurora arc, from which the substorm poleward expansion was initiated. Three of these events are shown bellow.

3.2.1. The 5 April 2009 Event

[12] The spacecraft observations from 06:55 to 07:15 UT on 5 April 2009 are summarized in Figure 2, with THD shown in Figure 2 (top) and THE shown in Figure 2 (bottom). The energy spectrograms, pressures including thermal pressure, magnetic pressure, total pressure and equatorial plasma pressure, magnetic field, bulk velocity and perpendicular velocity are shown for both spacecraft. Magnetic β is shown for THD, which is located in the central plasma sheet. The magnetic β observed by THE was large during the early growth phase but reduced substantially due to THE moving out of the plasmas sheet before onset. The substorm onset was identified at 07:04:54 UT (red vertical dashed line). During the growth phase, the plasma sheet was highly stretched as can be seen from the extremely low B_z. The equatorial pressure slightly increased starting ~4 min before the substorm onset, with the enhancement being larger at the more duskward spacecraft THE. This pressure increase is associated with the ion energy flux enhancement in the ~5 to ~10 keV range, and

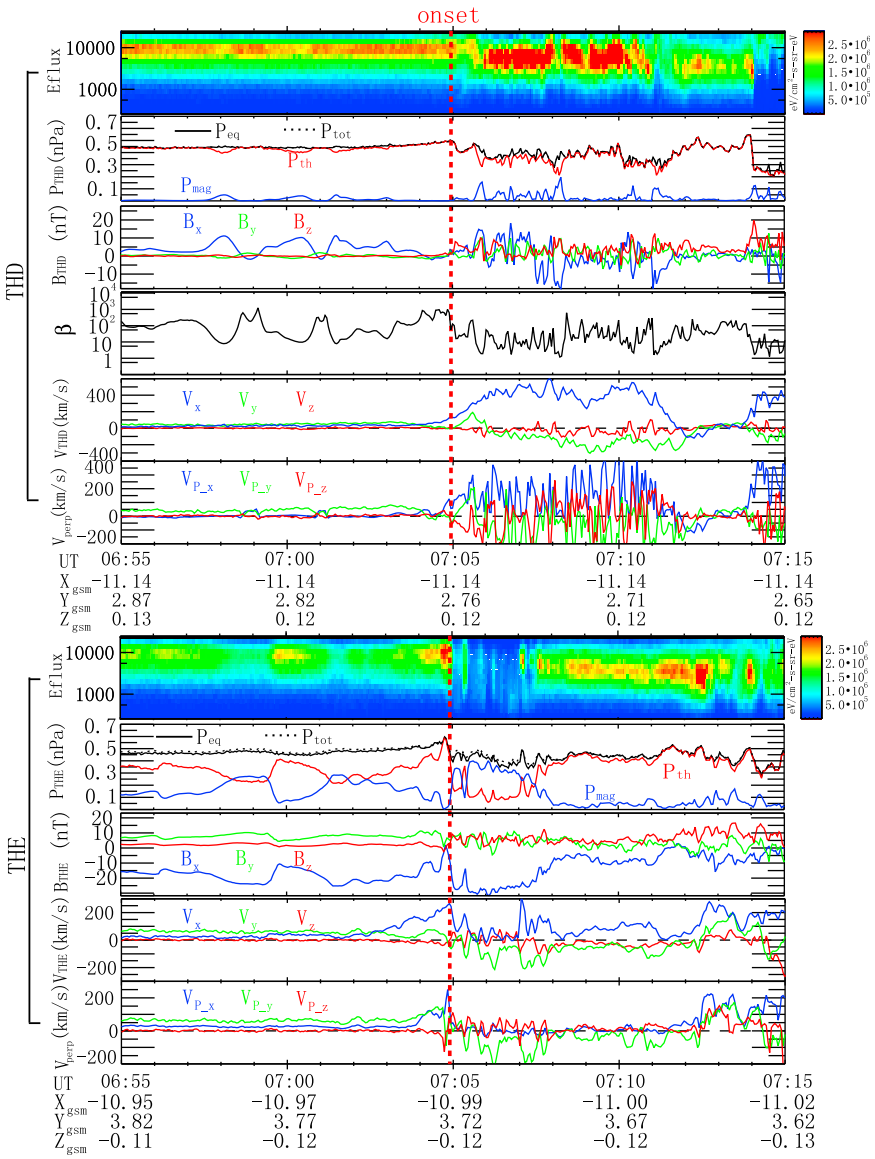

Figure 2. (top) THD observations: ion energy flux; thermal pressure (red curve), magnetic pressure (blue curve), equatorial plasma pressure (solid black line), and total pressure (dashed black line); magnetic field; magnetic β; ion bulk flow; and perpendicular flow. (bottom) THE observations are in a similar format as those for THD, excluding magnetic β on 5 April 2009 between 06:55:00 and 07:15:00 UT.

substantial westward flows. From ~1 min before onset, the earthward and duskward flow at THE location strongly enhanced associated with an energy flux increase near 10 keV, while the duskward flows at THD reduced. This pattern is seen in two of our events, but not the others.

[13] Figure 3 displays contours of the ion distribution function in the plane perpendicular to the magnetic field with the velocities projected into the X_{GSM} - Y_{GSM} plane from THD (left) and THE (right) at ~07:04:30 UT. The white dash circles indicate energies of ~1 keV, ~5 keV and ~10 keV. The distribution observed by THD does not show substantial shift in velocity, which is consistent with the small perpendicular velocity shown in Figure 2. THE shows a weak distribution shift corresponding to earthward velocity for lower-energy ions at one to several keV, and a strong distribution shift corresponding to earthward and westward velocity at energies from about several keV and above. The energy dependence of the duskward flow shift is a signature that is expected from magnetic drift.

[14] The spacecraft footprints were mapped to the vicinity of the THEMIS ground based ASI station at Fort Smith (FSMI). Figure 4 shows selected images near the center FSMI field-of-view (FOV) during the late growth phase, with cyan and blue squares representing the footprints of spacecraft THD and THE, respectively, mapped by using the T96 magnetic field model using 2 h averaged solar wind as input (obtained from OMNIWeb high-resolution data). The dashed rectangle in the first plot of Figure 4 represents

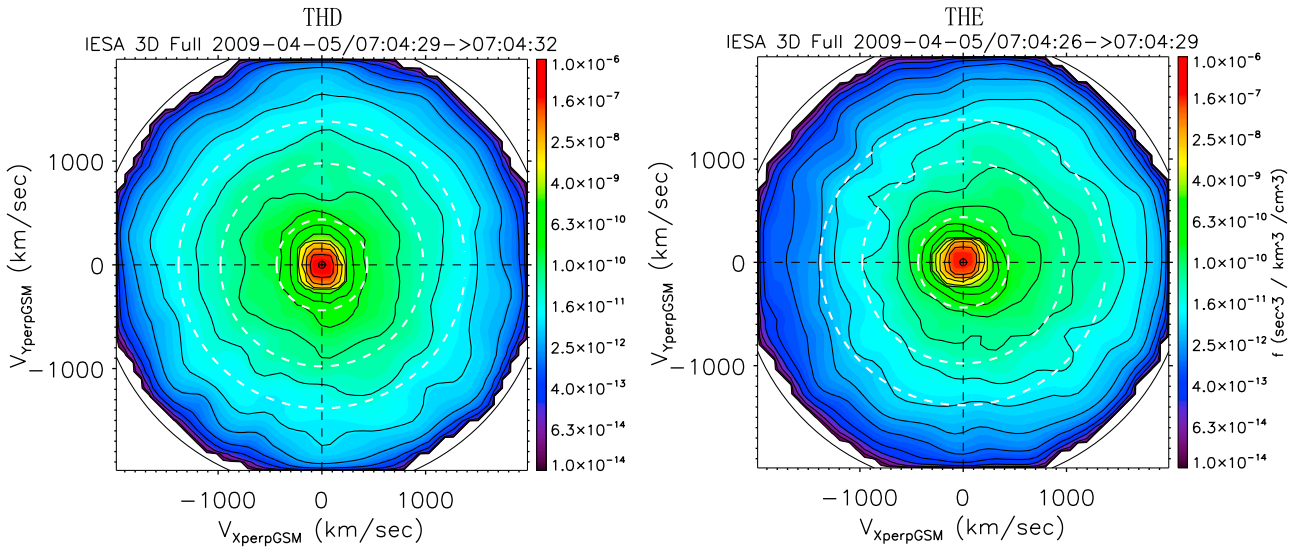

Figure 3. Two-dimensional ion distribution from (left) THD and (right) THE in the plane perpendicular to magnetic field with *x* axis projected from X_{GSM} and *y* axis projected from Y_{GSM} at ~07:04:30 UT on 5 April 2009.

the possible range of the footprint of THD using extremum solar wind conditions during the 2 h before the substorm onset. The cyan and blue circles represent the footprints of THD and THE mapped by the T01 magnetic field model using instantaneous solar wind input. The T96 model maps the spacecraft footprints closer to the aurora arc that developed simultaneously with the spacecraft observations (shown below). Thus we consider the more highly stretched T96 model to be the better model for field line tracing for the growth phase conditions considered here.

[15] Ignoring the moon light in the lower left portion of the FOV, a thin arc appeared at ~07:01 UT and gradually intensified after ~07:02:30 UT near the latitudinal center of the FOV. The substorm onset brightening initiated from this arc toward the west of the FOV at ~07:04:54 UT. There was another weak wider arc located slightly poleward of the onset arc, but its intensity did not noticeably change during the entire late growth phase, suggesting that this more poleward arc did not affect the occurrence of the onset.

[16] In Figure 5, the azimuthal pressure gradient calculated from P_{THD}-P_{THE} by using the equatorial plasma pressure shown in Figure 2, and ground-based keograms from FSMI are stacked together. The first plot in Figure 5 shows that the azimuthal pressure gradient was very small ~10 min before onset with moderate oscillations, and similar small gradient were found over the entire 30 min growth phase period (not shown here). Starting ~2.5 min before onset, the pressure gradient started to increase toward negative values (which means duskward), and experienced a sharp increase starting ~1 min before onset. According to the Vasyliunas equation [*Vasyliunas*, 1970], enhanced duskward pressure gradient with the flux tube volume gradient dominantly radially outward gives enhanced upward FAC from the ionosphere.

[17] The second and third plots of Figure 5 also shows the white light keograms from the camera center-west FOV (~0.36 MLT to the west of the center) and the center FOV. The auroral poleward expansion was initiated at 07:04:54 UT near the camera center-west view, and expanded azimuthally to the center FOV ~1 min later. A thin arc, from which the poleward expansion occurred, started to intensify ~2.5 min before the onset time at the center FOV near 66.8° MLAT (highlighted by the yellow arrow), and extended westward to the onset meridian before onset. The intensification of this arc occurred nearly simultaneously with the duskward pressure gradient enhancement, suggesting correlation between the enhanced upward FAC associated with the arc intensification and that with the enhanced duskward pressure gradient. This arc intensification is also consistent with the preonset intensification of the onset arc found by *Lyons et al.* [2002], which is formed equatorward of the growth phase arcs a few minutes before onset.

[18] The fourth through the sixth plots in Figure 5 are multispectral keograms from NORSTAR meridian scanning photometer (MSP) data at wavelengths 557.7 nm, 630.0 nm, and 486.1 nm (H_β) along the FSMI central meridian. The 557.7 nm emission shows a thin arc intensification centered at ~66.8° MLAT starting from ~2.5 min before onset, which exactly corresponds to the white light arc during the late growth phase. This intensification is consistent with the hard electron emission found by *Voronkov et al.* [2003] during the several minutes time interval before substorm onset. The 630.0 nm emission shows a similar arc of much weaker intensity than the 557.7 nm emissions, indicating that the onset electron auroral arc is related to both hundreds of eV and >1 keV electrons, with the harder electron precipitation dominant. The enhanced energy flux of the electron precipitation, inferred from the arc intensification, is the expected result of the enhanced field-aligned potential drop caused by the enhanced upward FAC associated with the increasing duskward pressure gradient. The weak H_β emission shows a persistent diffuse pattern before onset

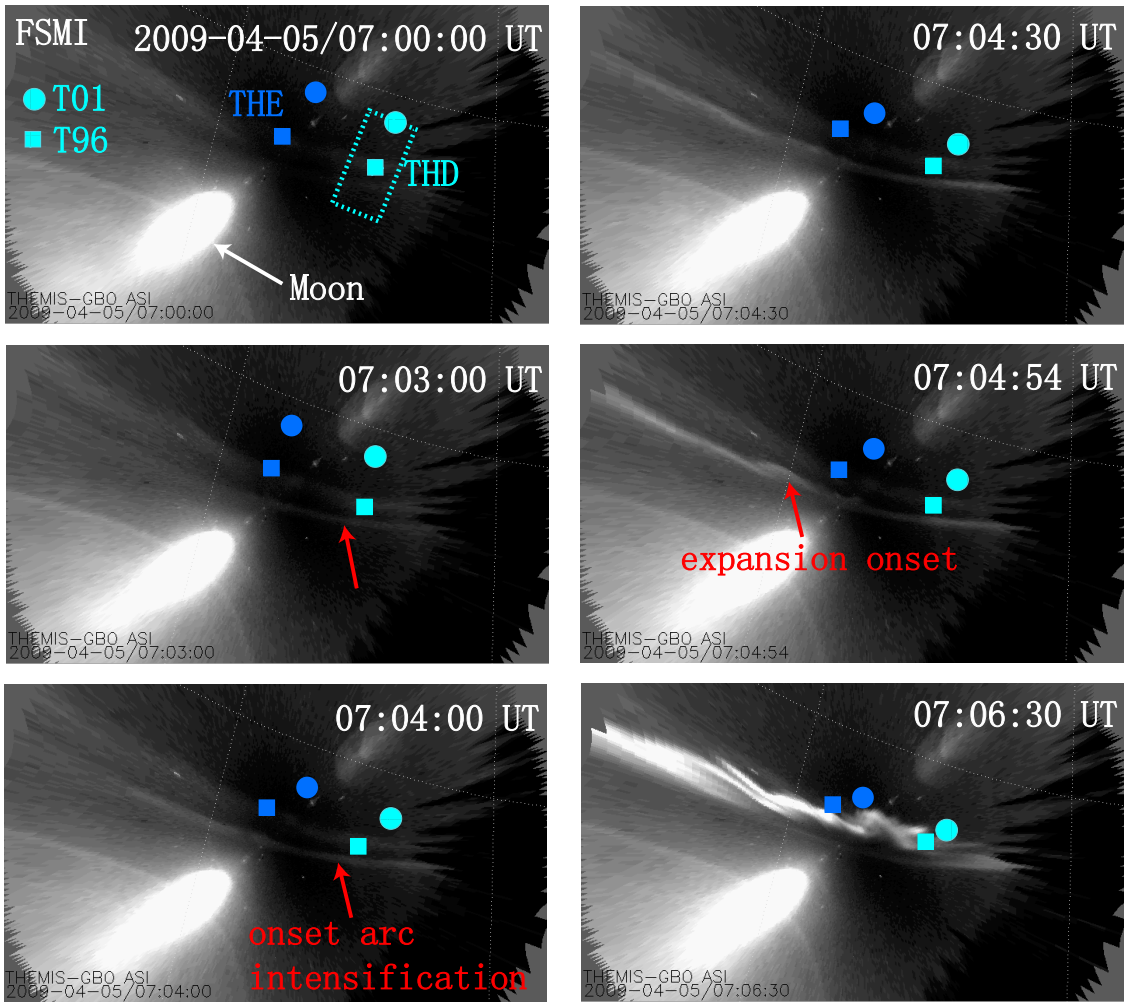

Figure 4. Selected white light auroral images from the FSMI All-Sky Imager before the substorm onset on 07:04:54 UT on 5 April 2009. The cyan and blue squares represent the footprints of THD and THE mapped by T96 magnetic field model by using 2 h averaged solar wind conditions. The dashed cyan rectangle represents the THD footprint range by using extremum solar wind conditions in 2 h as T96 input. The cyan and blue circles represent the footprints of THD and THE mapped by T01 magnetic field model using instantaneous solar wind conditions as input.

with its peak region located equatorward of the electron aurora arc, which is consistent with growth phase arc properties observed by *Deehr and Lummerzheim* [2001] and *Lessard et al.* [2007]. The H_β emission does not display a substantial arc intensification, which confirms that the white light arc intensification during the late growth phase in our event is the electron aurora.

3.2.2. The 19 March 2009 Event

[19] The second event on 19 March 2009 shows similar preonset pressure changes. Figure 6 displays the spacecraft observations from THD and THE in the upper and lower portions, respectively, from 06:30 to 07:10 UT, with the substorm onset occurring at ~06:51 UT. Shown in Figure 6 are (from top to bottom): pressures in the same format as those in Figure 2, magnetic fields, perpendicular velocities, and magnetic β for THD. The equatorial plasma pressure in solid black line shows a gradual increase ~10 min before onset at both spacecraft locations. This enhancement started to become larger at THE ~5 min before the onset, which is not observed at THD. During the entire 20 min before onset, the magnetic field was highly stretched. The energy flux data are not comparable between these two spacecraft due to THE moving off equatorial plane. Nevertheless, the ion duskward flow was sustainably larger at THE than that at THD near the center plasma sheet within ~10 min before onset. The magnetic β increased to over 50 and underwent strong fluctuations several minutes before onset, which is similar to the first event above. The ion distribution function with the Y_{GSM} and Z_{GSM} projected on the perpendicular plane shown in Figure 7 from the two spacecraft show also the energy-dependent duskward drift, indicating stronger duskward magnetic drift at the more duskward location during the growth phase.

[20] During the late growth phase, the spacecraft footprints were mapped to the vicinity of the THEMIS ASI at Gilliam (GILL) where the onset expansion was observed.

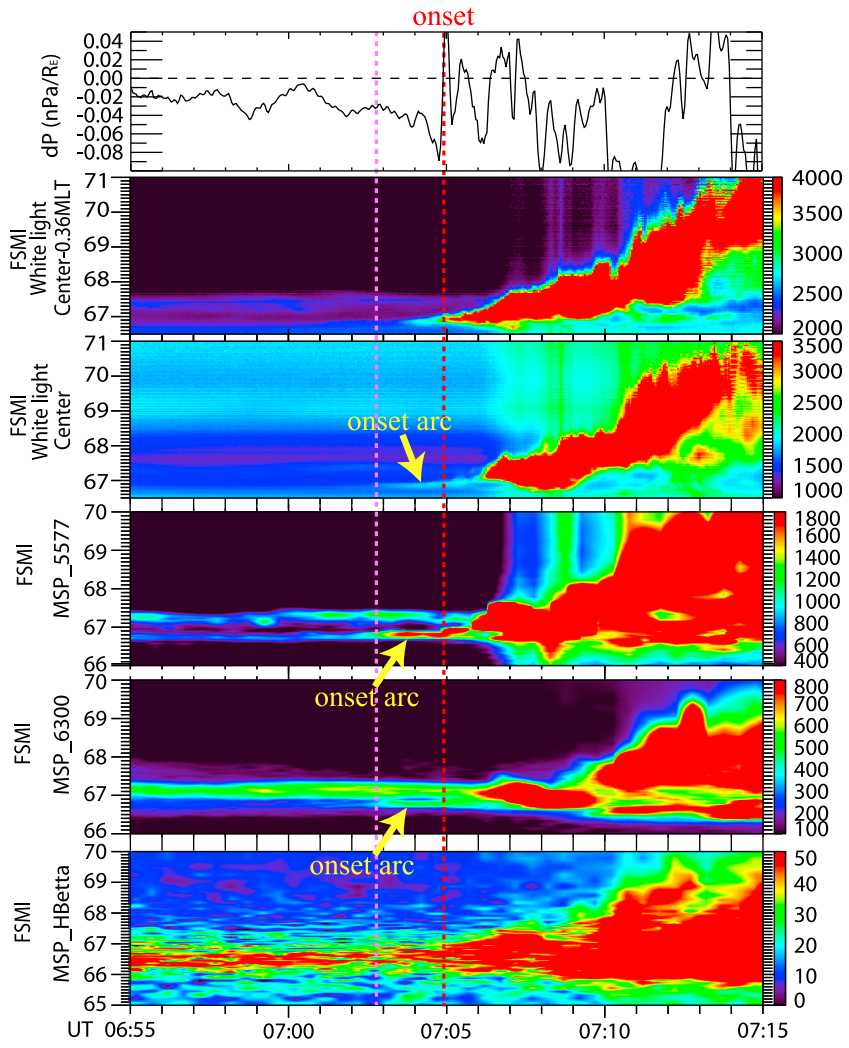

Figure 5. (top to bottom) Equatorial plasma pressure gradient, auroral white light keogram from FSMI center-west FOV, white light keogram from FSMI center FOV, auroral 557.7 nm emission from FSMI center FOV, 630.0 nm emission, and 486.1 nm between 06:55:00 and 07:15:00 UT on 5 April 2009. The dashed magenta line identifies the initiation of the pressure gradient enhancement.

Figure 8 shows six selected snapshots zoomed in to the center of the GILL FOV. The onset arc started to intensify ~5 min before onset, as can be observed in the eastern portion of the GILL FOV, and then extended westward near the auroral oval equatorward boundary. Multi-image observations show that this arc extended more eastward over 2 MLT to the SNKQ FOV (not shown here), and an eastward gradient of brightness along the onset arc is visible in the arc as it extended westward. At the same time, another arc located more poleward and westward of the onset arc started to move equatorward and could be connected to a preonset aurora streamer structure as considered by *Nishimura et al.* [2010a]. The substantial duskward flow and very minor earthward flow observed by the spacecraft indicate that the plasma sheet temporal changes at the spacecraft location should be related to the westward expanded onset arc rather than the equatorward moving poleward arc. The onset occurred in the western portion of the GILL FOV where the two arcs moved close together. This substorm event is not an entirely isolated onset. A pseudobreakup occurred near the onset location ~30 min before onset, and a ~5 min arc azimuthal shear was found ~2° poleward of the onset arc ~20 min before onset. However, the timing and the location of these activities did not show any direct relation with the onset arc intensification. Thus we suggest that the onset arc intensification and the near-Earth plasma sheet variations prior to onset are not consequent changes of the previous activities.

[21] Figures 9a and 9b display the azimuthal pressure gradient and the GILL multispectral keograms at different longitudes between 06:40 and 07:00 UT. The first plots in Figures 9a and 9b show a strong duskward enhancement of the azimuthal pressure gradient initiating ~5 min before onset, indicating enhanced upward FAC. The onset poleward expansion can be identified starting from ~06:51 UT from both the white light and the 630.0 nm emission keograms in the GILL center-west FOV as shown in the second

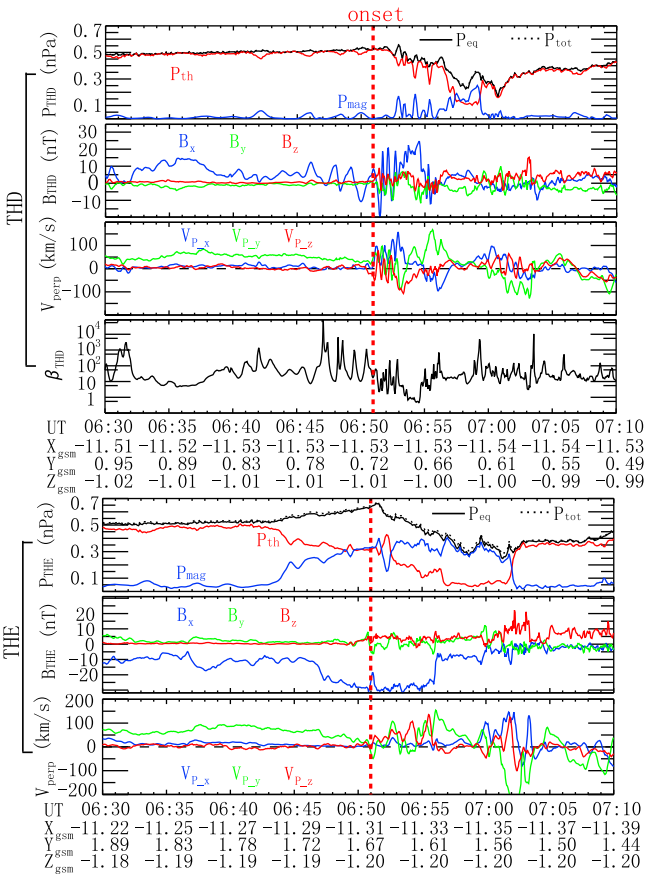

Figure 6. THEMIS spacecraft data from (top) THD and (bottom) THE between 06:30:00 and 07:10:00 UT on 19 March 2009, respectively. Pressures (same color code as in Figure 1), magnetic field, and perpendicular velocity are shown. Also shown is the central plasma sheet magnetic β obtained from THD.

and third plots of Figure 9a. The equatorward moving more poleward arc can also be identified extending from ~66.5° MLAT to ~66° MLAT during the whole 10 min before onset at this longitude. The onset arc is observed to intensify ~5 min before onset at ~66° MLAT by both the white light and the 630.0 nm keograms in the GILL center-east FOV as shown in the fourth and fifth plots of Figure 9a, which is at exactly the same time as the duskward pressure gradient enhancement, and suggests that the electron arc results from the enhanced upward FAC associated with enhancing pressure gradient. This also suggests that the spacecraft footprints should be mapped slightly more eastward than those shown in Figure 8.

[22] Figure 9b stacks the same pressure gradient data with the MSP data at GILL center FOV. Both white light and 557.7 nm emission show that the onset arc extended to this longitude and connected with the equatorward moving arc ~1 min before onset. The onset arc at 630.0 nm emission is weaker than the 557.7 nm emission, which suggests that the strong duskward pressure gradient associated with upward FAC led to precipitation with keV electrons dominant. While 557.7 nm emission data is only available along the central meridian during this event, the same arc is observed in both white light and 630.0 nm at the more eastward longitude that we suggest maps closet to the spacecraft. Thus it is likely that the onset arc at the camera center-east meridian was also more intense in 557.7 nm than at 630.0 nm. The proton aurora in the fifth plot of Figure 9b does not show a substantial intensification as electron aurora does, but a small and noisy increase, consistent with the enhanced upward FAC doing changes to electrons. It is difficult to reliably connect this small increase to the proton flux increase associated with the pressure gradient increase. The onset arc is located within the proton arc, consistent with our mapping of the electron arc brightening associated with the pressure changes observed within the plasma sheet.

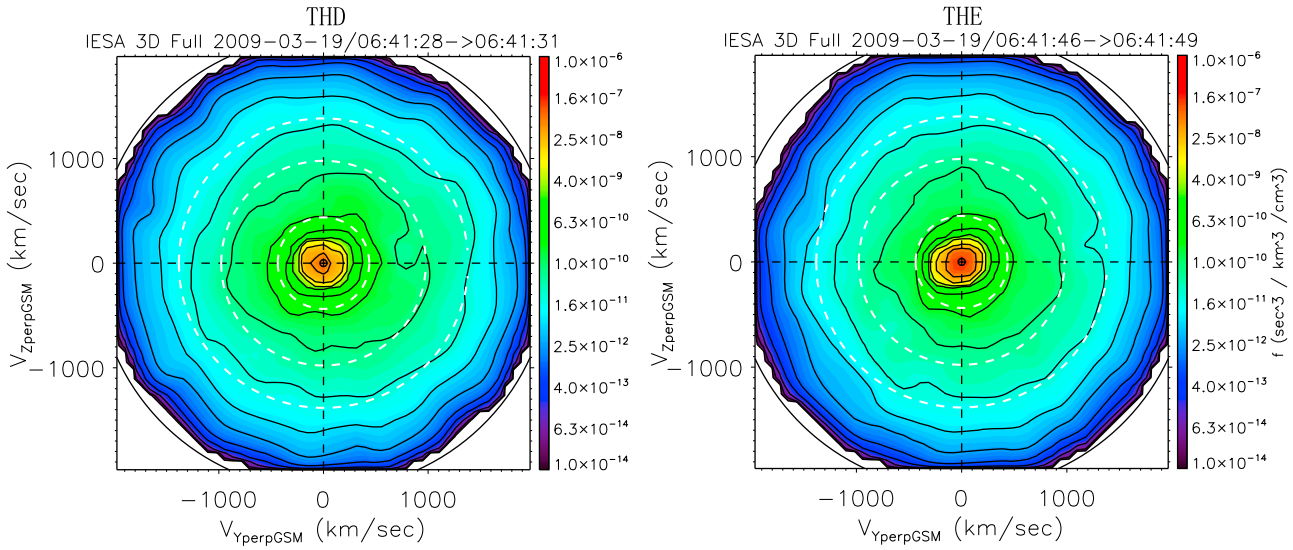

Figure 7. Two-dimensional ion distribution from (left) THD and (right) THE in the same plane as those in Figure 3 at ~06:41:40 UT on 19 March 2009.

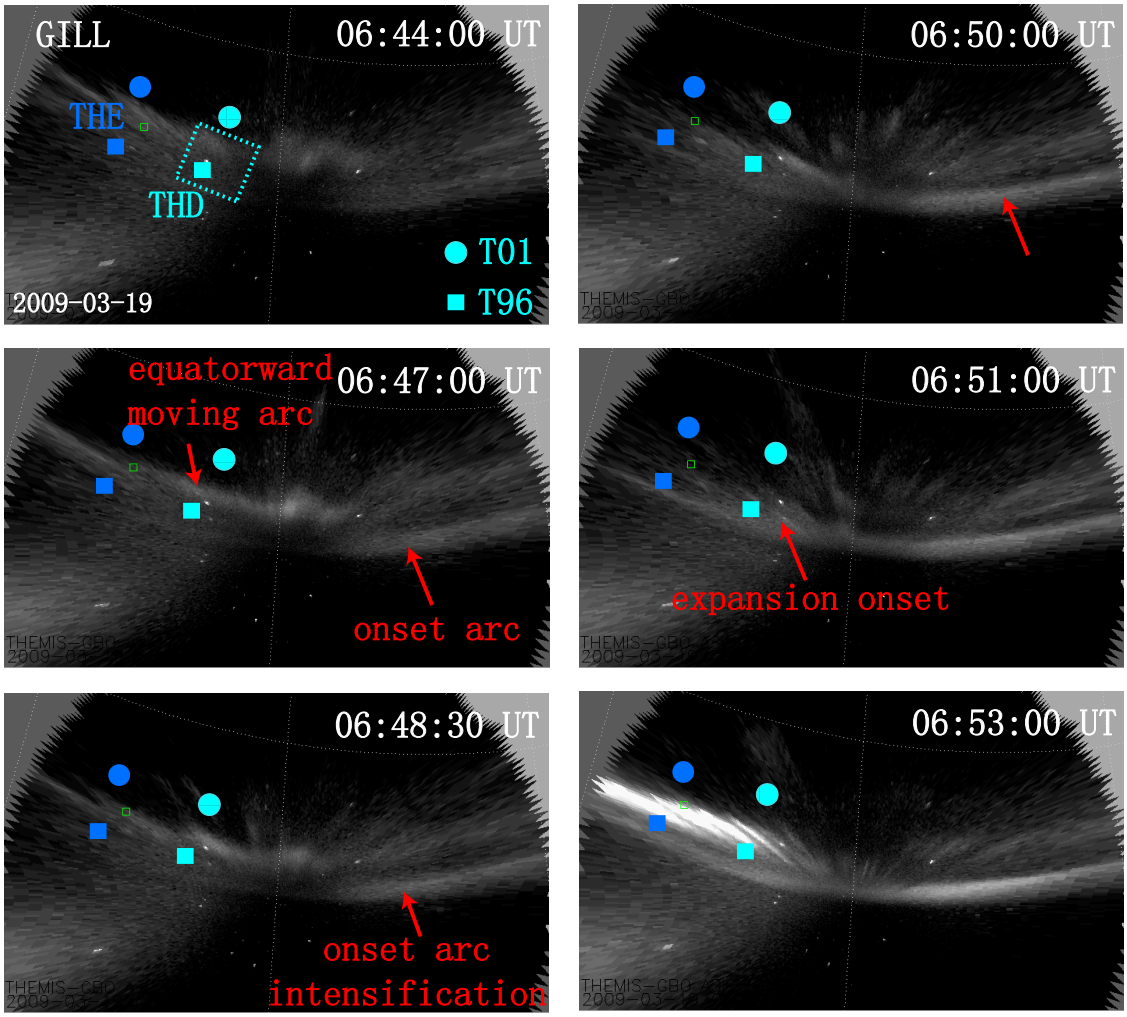

Figure 8. Selected white light auroral images from the GILL All-Sky Imager before the substorm onset at 06:51:00 UT on 19 March 2009.

3.2.3. The 29 March 2009 Event

[23] Consistent features were also found in the third substorm event on 29 March 2009. Figure 10 shows the ion energy flux, pressures, magnetic field and perpendicular flow from the spacecraft THD in the upper portion, and the same quantities together with magnetic β from THE in the lower portion between 04:50:00 and 05:40:00 UT. The growth phase plasma sheet within half an hour before onset is quite steady with the ion energy peaks between 5 and 10 keV. The central plasma sheet pressure remains almost constant, and the field line is highly stretched. Starting ~10 min before onset, THD gradually moved into the northern plasma sheet, while THE still stayed very close to the neutral sheet. THE observed a sharp small amplitude pressure increase ~2 min before onset, which was associated with an enhanced earthward and duskward perpendicular flow, which are not observed by THD. The distribution functions show stronger energy-dependent duskward flow by THE than that by THD (not shown here). These are similar as seen for the first event shown in Figures 2 and 3. The magnetic β observed by THE in this case stayed as high as ~100, and strongly increased ~2 min before onset as pressure increased.

[24] Figure 11 shows, from top to bottom, the azimuthal pressure gradient, auroral white light and multispectral auroral keograms at 557.7 nm, 630.0 nm and H_β emissions between 05:05:00 and 05:25:00 UT. The pressure gradient gradually turned toward dawnward during 05:05 to 05:15 UT. This trend was reversed ~2 min before onset, where the pressure gradient experienced a moderate enhancement toward dusk. This duskward change may indicate a reverse of FAC from downward to upward contribute from azimuthal pressure gradient. The enhancement of the upward current may be smaller than for the previous two events owing to the smaller pressure gradient amplitude.

[25] The white light keogram does not show any clear pre-onset arc intensification possibly due to the light contamination overwhelming the arc intensity during the whole growth phase. The 557.7 emission shows a very weak and scattered enhancement ~1 min before onset. The 630.0 emission displays a moderate enhancement starting ~2 min before onset,

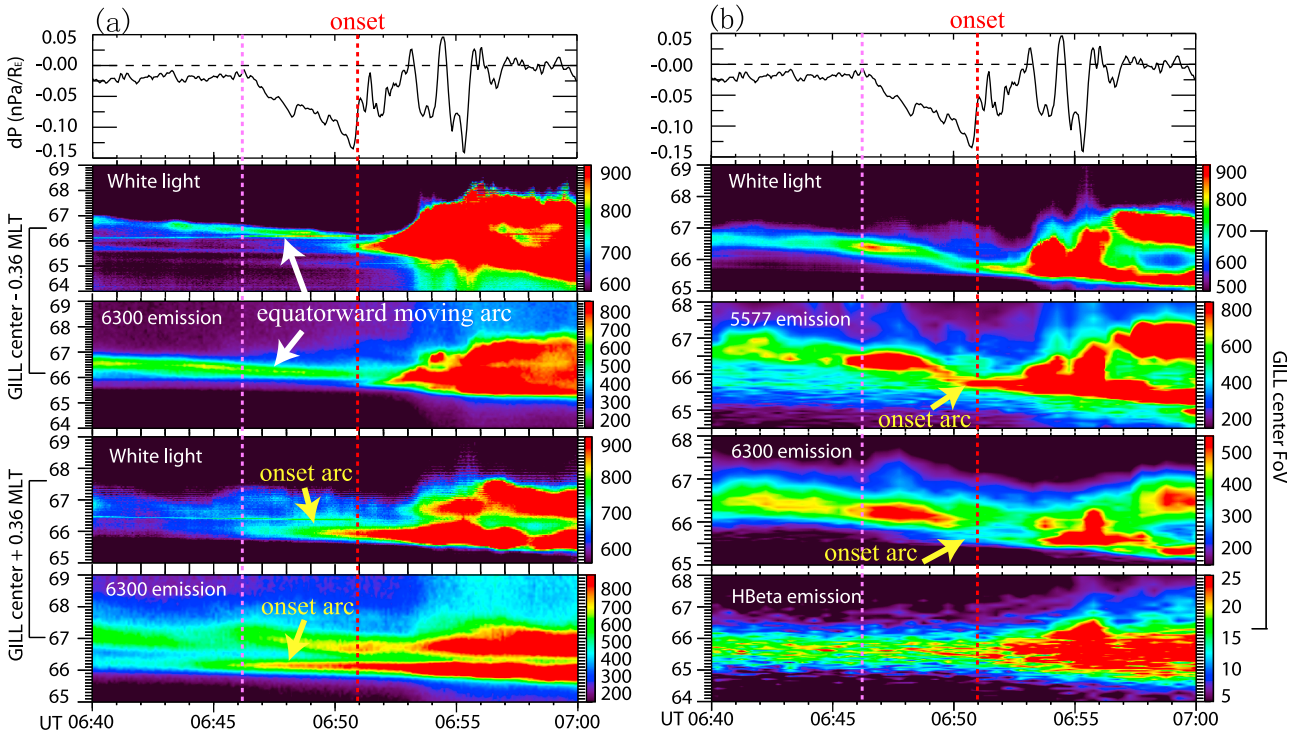

Figure 9. (a) (top to bottom) Equatorial plasma pressure gradient, auroral white light from GILL center-west FOV, 630.0 nm emission keograms from GILL center-west FOV, white light from GILL center-east FOV, and 630.0 nm emission keograms from GILL center-east FOV. (b) (top to bottom) White light, MSP 557.7 nm emission, 630.0 nm emission, and H_β emission from GILL center FOV on 19 March 2009 between 06:40:00 and 07:00:00 UT.

which is consistent with the pressure gradient change, although it covers a wider range in latitude than the previous two events. We suspect that the weak upward FAC driven by moderate duskward pressure gradient is not able to provide large enough field-aligned potential drop to energize the precipitating electrons up to the keV energy range. Thus in this case the soft electron precipitation dominants the preonset arc intensification during the late growth phase. Comparing with the H_β emission keogram in the fifth plot of Figure 11, the soft electron precipitation is again located within the poleward of the proton precipitation region, and there may have been some weak proton aurora intensification, though there is added uncertainty because atmospheric scattering seems to be somewhat stronger for this event than that for the previous events.

[26] It should be noticed that for balancing the azimuthal pressure changes in the near-Earth plasma sheet, the magnetic field has to change with the plasma redistribution, which would lead to the changing of azimuthal flux tube volume gradient. Combined with the strong earthward pressure gradient, this term will also contribute to FAC in a direction depending on the flux tube volume gradient direction. It should also be noted that radial pressure gradient temporal evolution could exist simultaneously with the azimuthal pressure gradient evolution. Despite these limitations, the similarity between aurora responses and the duskward azimuthal pressure gradient enhancements are consistent with the pressure gradient enhancements being responsible for the onset arc brightening prior to onset. The other two cases of our five events show similar duskward pressure gradient enhancement associated with preonset arc intensification before substorm onset, thus supporting this inference.

4. Summary and Discussion

[27] We have investigated the plasma sheet azimuthal pressure gradient during the late growth phase in the near-Earth transition region by using data from azimuthally lined-up THEMIS spacecraft during the 2009 tail season. Strict criteria were applied for selecting substorm events that were observed in ground based auroral observations while the azimuthal pressure gradient can be accurately measured within the central plasma sheet near the onset meridian. The auroral onset arc was found to intensify simultaneously with this azimuthal pressure gradient enhancement during this period preceding auroral breakup. Electron precipitation >1 keV was found to be dominant for cases having stronger pressure gradient enhancement; and softer electron precipitation was dominant for the one case when the pressure gradient enhancement was more moderate. We suggest that this reflects the strength of the upward FAC being determined by the strength of the azimuthal pressure gradient, and the field-aligned potential drop that energizes the precipitation electrons increasing with the strength of the upward FAC.

[28] In this study, we have adopted the auroral breakup onset as the substorm onset time, which has been broadly used in recent years [e.g., *Lyons et al.*, 2002; *Voronkov et al.*,

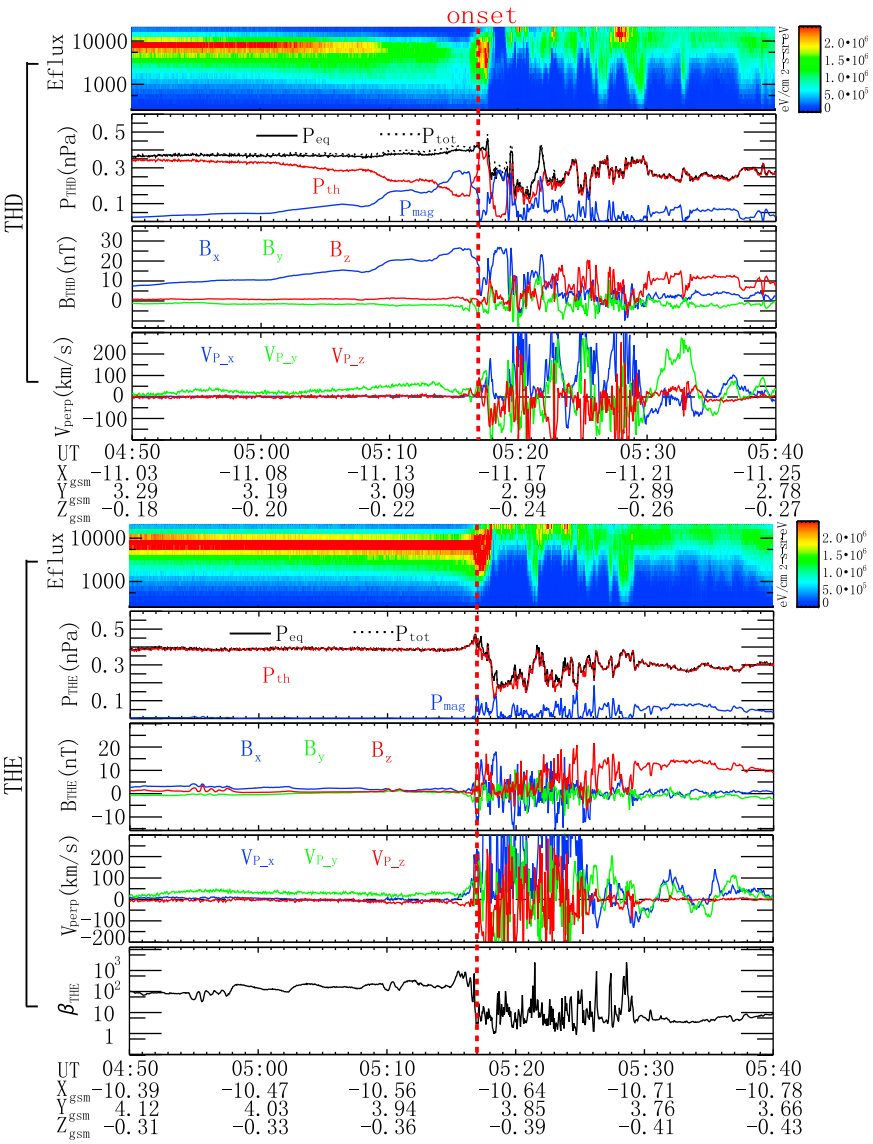

Figure 10. THEMIS spacecraft data from (top) THD and (bottom) THE. Ion energy flux, with pressures in the same color code as in Figure 2, magnetic field, and perpendicular velocity are shown. Also shown is magnetic β in the central plasma sheet between 05:05:00 and 05:25:00 UT on 29 March 2009.

2003; *Mende et al.*, 2008; *Nishimura et al.*, 2010b]. This makes the onset time easier and more accurately defined [*Mende et al.*, 2007] than using the initiation of gradual onset arc brightening before breakup. However, the several-minute thin arc brightening before poleward expansion could be the first stage of the substorm onset. Regardless of the definition of the onset time, our study reflects the plasma sheet evolution corresponding to the gradual auroral enhancement before the explosive stage.

[29] Our observations could be relevant to suggestions that have been presented for the substorm onset instability. For example, *Stepanova et al.* [2002] suggested that the azimuthal pressure gradient associated with enhanced FAC might lead to a modified interchange instability. Our results are consistent with this suggested process for substorm expansion onset. Also, *Antonova et al.* [2009] suggested that a gradual auroral enhancement as found here might lead to an electrostatic instability within the inner plasma sheet. It is also worth noting that pressure angular data (not shown) shows an enhancement of parallel pressure giving a field-aligned anisotropy $P_{\parallel} > P_{\perp}$ at THE for three of the five events, and at THD for one of the five events, in association with the spatial pressure gradient enhancement. This could be important for future study and might indicate that a localized thin sheet current formed near the center of the current sheet at the more duskward location [*Cowley*, 1978], suggesting that the tension force might also play some role in the plasma sheet force balance before onset.

[30] From another point of view, the timing of the pressure gradient enhancement is similar to that of the ~0.01 Hz magnetic oscillations that have been observed several minutes before onset dipolarizations [e.g., *Cheng and Lui*, 1998;

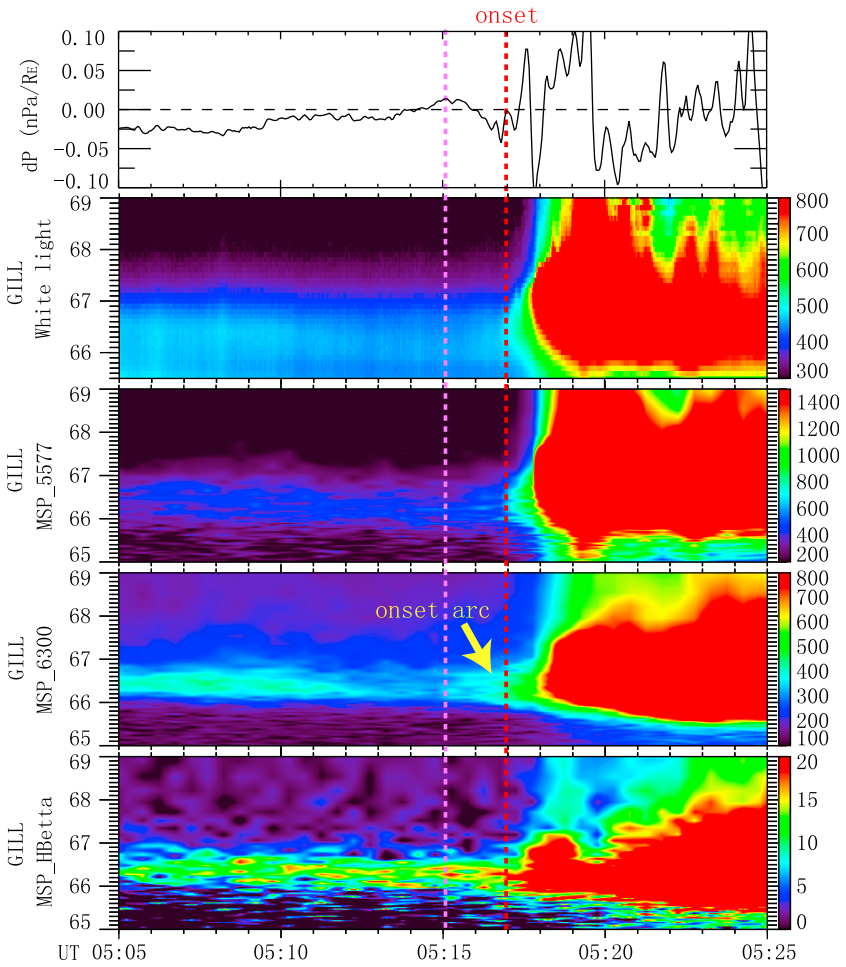

Figure 11. (top to bottom) Equatorial plasma pressure gradient, auroral white light, and 57.7 nm emission, 630.0 nm emission, and H_β emission keograms from GILL center FOV in the between 05:05:00 and 05:25:00 UT on 29 March 2009.

Saito et al., 2008; *Park et al.*, 2010]. Considering the very high β value observed in the case study, we may also speculate that the preonset azimuthal pressure gradient enhancement and the associated enhancement of the magnetic curvature might lead to growth of the ballooning mode instability, which could be closely related to preonset plasma kinetic effects [*Cheng and Lui*, 1998; *Cheng and Zaharia*, 2004]. However, it is not clear whether the preonset pressure gradient enhancement is a sufficient condition for onset instability or simply sets a necessary precondition for the intrusion of new low-entropy plasma to lead to instability [*Nishimura et al.*, 2010a; *Xing et al.*, 2010]. Thus our case study suggests that a preonset azimuthal pressure gradient buildup is common near the onset location within the inner plasma sheet, and this condition may be easily disturbed when the reduced entropy plasma is transported into the inner plasma sheet region. It is also possible that the preonset pressure gradient enhancement near the inner plasma sheet region that we have observed could be related to the pressure enhancement ahead of an earthward moving low-entropy flow channel [*Yang et al.*, 2011]. This transient azimuthal pressure gradient change before substorm onset should be further investigated using more detailed observations and instability analysis to determine the role it plays in leading to substorm onsets.

[31] **Acknowledgments.** This work at UCLA was supported by National Science Foundation grants ATM-0639312 and ATM-0646233 and NASA grant NNX09AI06G. THEMIS is funded by NASA contract NAS5–02099. Deployment of the THEMIS ASIs was partly supported by CSA contract 9F007–046101. OMNI solar wind data were provided through the Coordinated Data Analysis Web. We greatly thank James McFadden for providing THEMIS ESA data. We are grateful to Gang Lu and Xuzhi Zhou for helpful discussions.

[32] Masaki Fujimoto thanks Christian Jacquey and Marina Stepanova for their assistance in evaluating this paper.

References

Angelopoulos, V. (2008), The THEMIS mission, *Space Sci. Rev.*, *141*, 5–34, doi:10.1007/s11214-008-9336-1.

Angelopoulos, V., et al. (2008), Tail reconnection triggering substorm onset, *Science*, *321*, 931–935, doi:10.1126/science.1160495.

Antonova, E. E., I. A. Kornilov, T. A. Kornilova, O. I. Kornilov, and M. V. Stepanova (2009), Features of auroral breakup obtained using data of ground-based television observations: Case study, *Ann. Geophys.*, *27*, 1413–1422, doi:10.5194/angeo-27-1413-2009.

Auster, H. U., et al. (2008), The THEMIS fluxgate magnetometer, *Space Sci. Rev.*, *141*, 235–264, doi:10.1007/s11214-008-9365-9.

Bristow, W. A., and P. Jensen (2007), A superposed epoch study of SuperDARN convection observations during substorms, *J. Geophys. Res.*, *112*, A06232, doi:10.1029/2006JA012049.

Bristow, W. A., A. Otto, and D. Lummerzheim (2001), Substorm convection patterns observed by the Super Dual Auroral Radar Network, *J. Geophys. Res.*, *106*, 24,593–24,609, doi:10.1029/2001JA000117.

Bristow, W. A., G. Sofko, H. C. Stenbaek-Nielsen, S. Wei, D. Lummerzheim, and A. Otto (2003), Detailed analysis of substorm observations using SuperDARN, UVI, ground-based magnetometers, and all-sky imagers, *J. Geophys. Res.*, *108*(A3), 1124, doi:10.1029/2002JA009242.

Cheng, C. Z., and A. T. Y. Lui (1998), Kinetic ballooning instability for substorm onset and current disruption observed by AMPTE/CCE, *Geophys. Res. Lett.*, *25*, 4091–4094, doi:10.1029/1998GL900093.

Cheng, C. Z., and S. Zaharia (2004), MHD ballooning instability in the plasma sheet, *Geophys. Res. Lett.*, *31*, L06809, doi:10.1029/2003GL018823.

Cowley, S. W. H. (1978), The effect of pressure anisotropy on the equilibrium structure of magnetic current sheets, *Planet. Space Sci.*, *26*, 1037–1061, doi:10.1016/0032-0633(78)90028-4.

Deehr, C., and D. Lummerzheim (2001), Ground-based optical observations of hydrogen emission in the auroral substorm, *J. Geophys. Res.*, *106*, 33–44, doi:10.1029/2000JA002010.

Erickson, G. M., and R. A. Wolf (1980), Is steady convection possible in the Earth's magnetotail?, *Geophys. Res. Lett.*, *7*, 897–900, doi:10.1029/GL007i011p00897.

Gkioulidou, M., C.-P. Wang, L. R. Lyons, and R. A. Wolf (2009), Formation of the Harang reversal and its dependence on plasma sheet conditions: Rice convection model simulations, *J. Geophys. Res.*, *114*, A07204, doi:10.1029/2008JA013955.

Lessard, M. R., W. Lotko, J. LaBelle, W. Peria, C. W. Carlson, F. Creutzberg, and D. D. Wallis (2007), Ground and satellite observations of the evolution of growth phase auroral arcs, *J. Geophys. Res.*, *112*, A09304, doi:10.1029/2006JA011794.

Lui, A. T. Y. (2008), Comment on "Tail reconnection triggering substorm onset," *Science*, *324*, 1391, doi:10.1126/science.1167726.

Lui, A. T. Y., R. E. Lopez, B. J. Anderson, K. Takahashi, L. J. Zanetti, R. W. McEntire, T. A. Potemra, D. M. Klumpar, E. M. Greene, and R. Strangeway (1992), Current disruptions in the near-Earth neutral sheet region, *J. Geophys. Res.*, *97*, 1461–1480, doi:10.1029/91JA02401.

Lui, W. W., and G. Rostoker (1991), Effects of dawn-dusk pressure asymmetry on convection in the central plasma sheet, *J. Geophys. Res.*, *96*, 11,501–11,512, doi:10.1029/91JA01173.

Lyons, L. R., I. O. Voronkov, E. F. Donovan, and E. Zesta (2002), Relation of substorm breakup arc to other growth-phase auroral arcs, *J. Geophys. Res.*, *107*(A11), 1390, doi:10.1029/2002JA009317.

Lyons, L. R., et al. (2003), Substorm onset by plasma sheet divergence, *J. Geophys. Res.*, *108*(A12), 1427, doi:10.1029/2003JA010178.

Lyons, L. R., C.-P. Wang, M. Gkioulidou, and S. Zou (2009), Connections between plasma sheet transport, Region 2 currents, and entropy changes associated with convection, steady magnetospheric convection periods, and substorms, *J. Geophys. Res.*, *114*, A00D01, doi:10.1029/2008JA013743.

Lyons, L. R., Y. Nishimura, Y. Shi, S. Zou, H.-J. Kim, V. Angelopoulos, C. Heinselman, M. J. Nicolls, and K.-H. Fornacon (2010), Substorm triggering by new plasma intrusion: Incoherent-scatter radar observations, *J. Geophys. Res.*, *115*, A07223, doi:10.1029/2009JA015168.

McFadden, J. P., et al. (2008), The THEMIS ESA plasma instrument and in-flight 244 calibration, *Space Sci. Rev.*, *141*, 277–302, doi:10.1007/s11214-008-9440-2.

McPherron, R. L., C. T. Russell, and M. P. Aubry (1973), Satellite studies of magnetospheric substorms on August 15, 1968: 9. Phenomenological model for substorms, *J. Geophys. Res.*, *78*, 3131–3149, doi:10.1029/JA078i016p03131.

Mende, S. B., V. Angelopoulos, H. U. Frey, S. Harris, E. Donovan, B. Jackel, M. Syrjaesuo, C. T. Russell, and I. Mann (2007), Determination of substorm onset timing and location using the THEMIS ground-based observatories, *Geophys. Res. Lett.*, *34*, L17108, doi:10.1029/2007GL030850.

Mende, S. B., S. E. Harris, H. U. Frey, V. Angelopoulos, C. T. Russell, E. Donovan, B. Jackel, M. Greffen, and L. M. Peticolas (2008), The THEMIS array of ground-based observatories for the study of auroral substorms, *Space Sci. Rev.*, *141*, 357–387, doi:10.1007/s11214-008-9380-x.

Miyashita, Y., et al. (2009), A state-of-the-art picture of substorm-associated evolution of the near-Earth magnetotail obtained from superposed epoch analysis, *J. Geophys. Res.*, *114*, A01211, doi:10.1029/2008JA013225.

Nishimura, Y., L. Lyons, S. Zou, V. Angelopoulos, and S. Mende (2010a), Substorm triggering by new plasma intrusion: THEMIS all-sky imager observations, *J. Geophys. Res.*, *115*, A07222, doi:10.1029/2009JA015166.

Nishimura, Y., L. R. Lyons, S. Zou, X. Xing, V. Angelopoulos, S. B. Mende, J. W. Bonnell, D. Larson, U. Auster, and T. Hori (2010b), Pre-onset time sequence of auroral substorms: Coordinated observations by all-sky imagers, satellites, and radars, *J. Geophys. Res.*, *115*, A00I08, doi:10.1029/2010JA015832.

Ohtani, S., R. Yamaguchi, H. Kawano, F. Creutzberg, J. B. Sigwarth, L. A. Frank, and T. Mukai (2002), Does the braking of the fast plasma flow trigger a substorm? A study of the August 14, 1996, event, *Geophys. Res. Lett.*, *29*(15), 1721, doi:10.1029/2001GL013785.

Park, M. Y., D.-Y. Lee, S. Ohtani, and K. C. Kim (2010), Statistical characteristics and significance of low-frequency instability associated with magnetic dipolarizations in the near-Earth plasma sheet, *J. Geophys. Res.*, *115*, A11203, doi:10.1029/2010JA015566.

Saito, M. H., Y. Miyashita, M. Fujimoto, I. Shinohara, Y. Saito, K. Liou, and T. Mukai (2008), Ballooning mode waves prior to substorm-associated dipolarizations: Geotail observations, *Geophys. Res. Lett.*, *35*, L07103, doi:10.1029/2008GL033269.

Shiokawa, K., G. Haerendel, and W. Baumjohann (1998), Azimuthal pressure gradient as driving force of substorm currents, *Geophys. Res. Lett.*, *25*, 959–962, doi:10.1029/98GL00540.

Stepanova, M. V., E. E. Antonova, J. M. Bosqued, R. A. Kovrazhkin, and K. R. Aubel (2002), Asymmetry of auroral electron precipitations and its relationship to the substorm expansion phase onset, *J. Geophys. Res.*, *107*(A7), 1134, doi:10.1029/2001JA003503.

Stepanova, M. V., et al. (2004), Azimuthal plasma pressure reconstructed by using the Aureol-3 satellite date during quiet geomagnetic conditions, *Adv. Space Res.*, *33*, 737–741, doi:10.1016/S0273-1177(03)00641-0.

Tsyganenko, N. A. (2002a), A model of the near magnetosphere with a dawn-dusk asymmetry: 1. Mathematical structure, *J. Geophys. Res.*, *107*(A8), 1179, doi:10.1029/2001JA000219.

Tsyganenko, N. A. (2002b), A model of the near magnetosphere with a dawn-dusk asymmetry: 2. Parameterization and fitting to observations, *J. Geophys. Res.*, *107*(A8), 1176, doi:10.1029/2001JA000220.

Tsyganenko, N. A., and T. Mukai (2003), Tail plasma sheet models derived from Geotail particle data, *J. Geophys. Res.*, *108*(A3), 1136, doi:10.1029/2002JA009707.

Tsyganenko, N. A., and D. P. Stern (1996), Modeling the global magnetic field of the large-scale Birkeland current systems, *J. Geophys. Res.*, *101*, 27,187–27,198, doi:10.1029/96JA02735.

Vasyliunas, V. M. (1970), Mathematical models of magnetospheric convection and its coupling to the ionosphere, in *Particles and Fields in the Magnetosphere*, edited by B. M. McCormac, pp. 60–71, D. Reidel, Boston, Mass.

Voronkov, I. O., E. F. Donovan, and J. C. Samson (2003), Observations of the phases of the substorm, *J. Geophys. Res.*, *108*(A2), 1073, doi:10.1029/2002JA009314.

Wang, C.-P., L. R. Lyons, T. Nagai, and J. C. Samson (2004a), Midnight radial profiles of the quiet and growth-phase plasma sheet: The Geotail observations, *J. Geophys. Res.*, *109*, A12201, doi:10.1029/2004JA010590.

Wang, C.-P., L. R. Lyons, M. W. Chen, and F. R. Toffoletto (2004b), Modeling the transition of the inner plasma sheet from weak to enhanced convection, *J. Geophys. Res.*, *109*, A12202, doi:10.1029/2004JA010591.

Wang, C.-P., L. R. Lyons, T. Nagai, J. M. Weygand, and R. W. McEntire (2007), Sources, transport, and distributions of plasma sheet ions and electrons and dependences on interplanetary parameters under northward interplanetary magnetic field, *J. Geophys. Res.*, *112*, A10224, doi:10.1029/2007JA012522.

Wing, S., and P. Newell (1998), Central plasma sheet ion properties as inferred from ionospheric observations, *J. Geophys. Res.*, *103*, 6785–6800, doi:10.1029/97JA02994.

Wing, S., and P. Newell (2000), Quiet time plasma sheet ion pressure contribution to Birkeland currents, *J. Geophys. Res.*, *105*, 7793–7802, doi:10.1029/1999JA900464.

Wing, S., J. W. Gjerloev, J. R. Johnson, and R. A. Hoffman (2007), Substorm plasma sheet ion pressure profiles, *Geophys. Res. Lett.*, *34*, L16110, doi:10.1029/2007GL030453.

Xing, X., L. R. Lyons, V. Angelopoulos, D. Larson, J. McFadden, C. Carlson, A. Runov, and U. Auster (2009), Azimuthal plasma pressure gradient in quiet time plasma sheet, *Geophys. Res. Lett.*, *36*, L14105, doi:10.1029/2009GL038881.

Xing, X., L. Lyons, Y. Nishimura, V. Angelopoulos, D. Larson, C. Carlson, J. Bonnell, and U. Auster (2010), Substorm onset by new plasma intrusion: THEMIS spacecraft observations, *J. Geophys. Res.*, *115*, A10246, doi:10.1029/2010JA015528.

Yang, J., F. R. Toffoletto, R. A. Wolf, and S. Sazykin (2011), RCM-E simulation of ion acceleration during an idealized plasma sheet bubble injection, *J. Geophys. Res.*, *116*, A05207, doi:10.1029/2010JA016346.

Zou, S., L. R. Lyons, C.-P. Wang, A. Boudouridis, J. M. Ruohoniemi, P. C. Anderson, P. L. Dyson, and J. C. Devlin (2009), On the coupling between the Harang reversal evolution and substorm dynamics: A syn-

thesis of SuperDARN, DMSP, and IMAGE observations, *J. Geophys. Res.*, *114*, A01205, doi:10.1029/2008JA013449.

V. Angelopoulos, IGPP/ESS, University of California, Los Angeles, CA 90095-1567, USA.

U. Auster, Institut für Geophysik und Extraterrestrische Physik, Technische Universität Braunschweig, D-38106 Braunschweig, Germany.

C. Carlson and D. Larson, Space Sciences Laboratory, University of California, Berkeley, CA 94720-7450, USA.

E. Donovan, J. Liang, and E. Spanswick, Department of Physics and Astronomy, University of Calgary, 2500 University Dr., Calgary, AB T2N 1N4, Canada.

L. R. Lyons, Y. Nishimura, and X. Xing, Department of Atmospheric and Oceanic Science, University of California, Los Angeles, CA 90095-1567, USA. (xyxingchen@gmail.com)

Y. Nishimura, Solar-Terrestrial Environment Laboratory, Nagoya University, Furocho, Chikusa, Nagoya 464-8601, Japan.